*Pure Appl. Chem.*, Vol. 82, No. 11, pp. 2017–2025, 2010.
doi:10.1351/PAC-CON-09-12-03


# Possibilities of Monte Carlo simulation for examination of nanowhisker growth*

Alla G. Nastovjak, Igor G. Neizvestny, and Nataliya L. Shwartz‡

*Institute of Semiconductor Physics SB RAS, Novosibirsk, Russia*

*Abstract*: The kinetic Monte Carlo (MC) model of nanowhisker (NW) growth is suggested. Two variants of growth are possible in the model—molecular beam epitaxy (MBE) and chemical vapor deposition (CVD). The effect of deposition conditions and growth regimes on the whisker morphology was examined within the framework of the vapor–liquid–solid (VLS) mechanism. A range of model growth conditions corresponding to NW and nanotube formation was determined. The suggested MC model was used for analyses of the morphology of the catalyst–whisker interface and for examination of Si–Ge whisker growth.

*Keywords*: chemical vapor deposition (CVD); molecular beam epitaxy (MBE); Monte Carlo model; nanowhiskers; simulation.

## INTRODUCTION

Increasing interest in semiconductor nanowhiskers (NWs)—filamentary crystals—is due to their possible applications in electronics, photonics, and the life sciences. Ordered arrays of Si NWs may serve as electron emitters in field emission displays, and single vertical whiskers are used as tips for atomic force microscopy [1]. Superlattices on the base of whiskers with axial heterojunctions may be used as injection lasers, 1D waveguides, etc. Core-shell nanowires are applied as high-performance field effect transistors [2–4]. NWs find a use for biological and chemical sensors [5–7]. The main advantage of NW sensors is high sensitivity—single-molecule detection is possible [5]. The small size of the nanowire devices not only enables very high sensitivity detection, but also allows for hundreds of individually addressable nanowire devices to be defined within a single chip [7].

The main mechanism of whisker growth is the vapor–liquid–solid (VLS) mechanism suggested by Wagner and Ellis [8] to explain micrometer-scale Si NW growth from metal-droplet catalysts by chemical vapor deposition (CVD). In the VLS crystal growth mechanism, the vapor phase is supplied in the form of precursors or by thermal decomposition of solids. Very often, Au is used as catalyst since Si and Au form eutectic alloy with a low melting temperature at about 360 °C. At growth temperatures, Au–Si alloy is in the liquid phase. Si deposition results in the supersaturation of eutectic drops with semiconductor material, leading to Si crystallization at the Au–Si interface. The diameter of nanowires is close to that of the catalyst nanoparticle. Some other mechanisms such as vapor–solid–solid (VSS), solid–liquid–solid (SLS), and oxide-assisted growth (OAG) have also been employed for nanowire growth [9–12].

Semiconductor NWs can be grown from various materials such as Si, Ge, GaAs, InAs, InP, etc. [13–17]. Not only Au can be used as catalyst for initiation whisker growth, but also Ti, Fe, Al, Cu, Pt,

*Paper based on a presentation at the 5th International Symposium on Novel Materials and Their Synthesis (NMS-V) and the 19th International Symposium on Fine Chemistry and Functional Polymers (FCFP-XIX), 18–22 October 2009, Shanghai, China. Other presentations are published in this issue, pp. 1975–2229.

‡Corresponding author: E-mail: nataly.shwartz@gmail.com

and some other metals [9,18–21]. Various methods are explored for NW synthesis, for instance, CVD, laser ablation, molecular beam epitaxy (MBE), and template-based methods [18,22–24]. Nowadays, the main technique for NW growth is CVD, since it allows growing whiskers in a wider range of temperatures, fluxes, and whisker diameters than MBE. Recently it was reported about CVD growth of ultralong and highly uniform single-crystalline Si NWs with millimeter-scale length (2.3 mm) and aspect ratio up to approximately 100 000 [25]. Lately, it was demonstrated that MBE can be successfully used for growing Si and GaAs NWs [23,26]. Depending on NW and catalyst materials and growth conditions, one can achieve a different NW morphology. NWs can be straight, curved, branched, and hollow [15,27–30]. The morphology has an influence on the electron-optical and mechanical properties of NWs so it is necessary to optimize their shape and sizes. The electron-optical and structural properties have been calculated using ab initio methods [31,32], and the growth kinetics has been studied analytically [33]. Monte Carlo (MC) simulation allows the study of both the kinetics and morphology of growing whiskers.

Using the MC technique, one can study growth kinetics in the system with sizes comparable with sizes of real objects, and duration of model processes corresponded to real ones. Besides MC simulation takes into account spatio-temporal fluctuations that may be important in the growth process. In this work, MC realization of NW growth according to VLS mechanism and simulation results demonstrating the influence of growth regimes on whisker morphology are presented.

## MONTE CARLO MODEL

Simulation of NW growth was carried out using the program package SilSim3D—the program for MC simulation of atomic processes in three-dimensional multicomponent surface layer of crystal substrates [34,35]. The SilSim3D package allows the simulation of systems containing up to seven components with different chemical natures and valence. It is possible to simulate growth processes by taking into account the chemical reactions with the formation of solid and volatile components. The simulated layer of up to $10^7$ atomic sites is assumed to overlie a semi-infinite crystal wafer. It is considered that the crystal has a diamond-like structure. There is a space of sites unoccupied by any particles above the given layer. In the lateral directions, cyclic boundary conditions are applied. The input parameters of the model processes are: temperature $T$(K); flux intensity $F$(ML/s); process type (MBE or CVD). The input parameters of the model structure: composition, crystallography, and orientation of the substrate; initial layer morphology; activation energies of possible elementary events. The possible elementary events in the model are adsorption, desorption, diffusion, and chemical reactions. We consider the following chemical reactions: transmutation $A \rightarrow B$, dissociation $A \rightarrow B + C$, association $A + B \rightarrow C$ and exchange $A + B \rightarrow C + D$. The probability of each event is a Boltzmann probability (exponential function of its activation energy). The original real-time-scale event-scheduling reversed algorithm is based on a calculation of the configuration time, i.e., the time of an atom being settled at a regular lattice site in a particular environment. Details of the algorithm realization are described in [35]. One of the main advantages of the reversed algorithm based on the calculation of the configuration time is that all events occur on the real time scale. If the actual energy parameters of various events are specified in the model, the kinetics of the simulated process is characterized by the time parameters corresponding to the real process.

Figure 1 illustrates the atomic mechanism of NW growth. Precursors containing semiconductor material are deposited on the surface with catalyst drops. Precursors dissociated into NW material and volatile products. Atoms of semiconductor material may incorporate the substrate or diffuse toward the drop, dissolve in it, and then crystallize at the drop–whisker interface. The following facts were taken into consideration: (1) catalyst drop weakly wets the substrate surface; (2) semiconductor material arrives at the drop by vapor flux and by diffusion via the substrate surface. Two possible growth processes are allowable in the model—MBE or CVD. When we consider CVD growth, the drop plays the role of chemical catalyst, and high supersaturation in the drop can be achieved. Semiconductor mat-

 

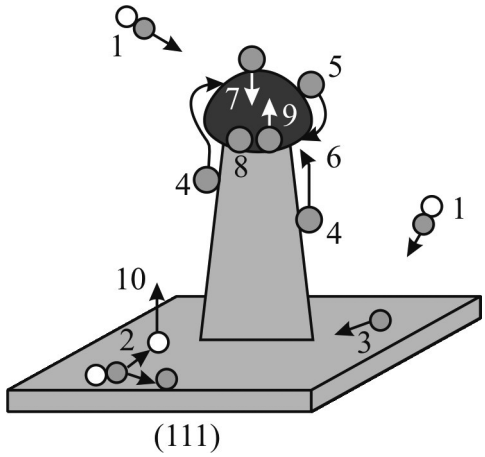


**Fig. 1** The scheme of the model system and considered processes: 1 – flux of precursor molecules; 2 – precursor dissociation; 3 – diffusion along the substrate surface; 4 – diffusion along NW wall; 5 – diffusion along catalyst drop surface; 6 – atom incorporation along the perimeter of the drop–whisker interface; 7 – dissolution of the semiconductor material in the drop; 8 – atom incorporation at the drop–whisker interface; 9 – atom detachment from interface and dissolution in the drop; 10 – evaporation of byproducts. The catalyst material is marked in dark gray, semiconductor material in light gray, and by-products in white.

ter in the form of precursors arrives to the surface at arbitrary angles imitating the vapor phase. If precursors easily desorb from non-activated semiconductor surface, the diffusion component of material flow to the drop is rather low. Simulation allows changing the diffusion component of growth in the CVD process, varying desorption properties of precursors. In the case of the MBE process, the whisker material is deposited in atomic form on the surface at definite angle. The drop surface does not play the role of chemical catalyst. It has only "ideal roughness" [36], which results in low supersaturation in the drop. Contrary to the CVD mode, the diffusion term is high in the growth mechanism.

Since our MC model is a lattice model, special effort was applied to imitate processes in a liquid drop. The surface tension of the drop was controlled by covalent bonding between catalyst atoms, and wetting was controlled by the binding energy between catalyst and whisker atoms. Lower bond energy corresponds to weaker wetting. In the lattice model, transport of semiconductor atoms within the liquid drop occurred by exchange diffusion by the following reaction: A + B $\rightarrow$ B + A, where A is a semiconductor material atom and B is an atom of the catalyst. Activation energy of the reaction depends on A and B atoms neighborhood. Due to diffusion, atoms of the semiconductor material reach the interface, where they could be incorporated into the growing facet or dissolved back into the drop. NWs grow layer by layer. The formation of a nuclei at the drop–whisker interface then is followed by the nuclei expansion in the lateral directions. Changing energy parameters of the system, we can consider different semiconductor-catalyst pairs.

The ranges of input parameters used for modeling in this work were: $T$ = 750–950 K, the intensity of precursor flux $F$ = (0.001 – 0.6) ML/s corresponds to experimental works [22,23], and catalyst drop diameters $d$ range between 3–20 nm in accordance with [13].

## SIMULATION RESULTS AND DISCUSSION

Depending on the ratio between adsorption and diffusion components, two different growth regimes can be considered: an adsorption- or diffusion-induced growth. There are two competitive ways for atoms to get at the drop–NW interface: diffusion through the drop followed by crystallization at the drop–whisker interface (the classical VLS mechanism) or incorporation along the triple line (incorpo-

ration regime). The relation between these two growth components depends on whisker diameter, the contact angle between the drop and the whisker, and solubility of the whisker material in the catalyst drop. It is possible to identify the growth mode by analyzing the growth rate dependence on catalyst drop diameter. Simulation results of growth rate dependence on drop diameter are presented in Fig. 2. In the diffusion-induced mode, if the growth is dominated by the classical VLS mechanism the growth rate is proportional to the inverse of the square of whisker diameter $d$ (Fig. 2a). But if the growth occurs mainly by incorporation via the triple line the growth rate is proportional to the inverse of $d$ (Fig. 2b). In the adsorption-induced mode, the growth rate is determined only by the external flux and is practically independent of the radius (Fig. 2c). Diameter-independent growth rate was demonstrated in CVD experiments [22], and ($1/d$)-dependence was revealed in MBE experiments [23,26]. Growth rate independence of diameter can be found only in the CVD process since in MBE growth, the diffusion component always dominates.

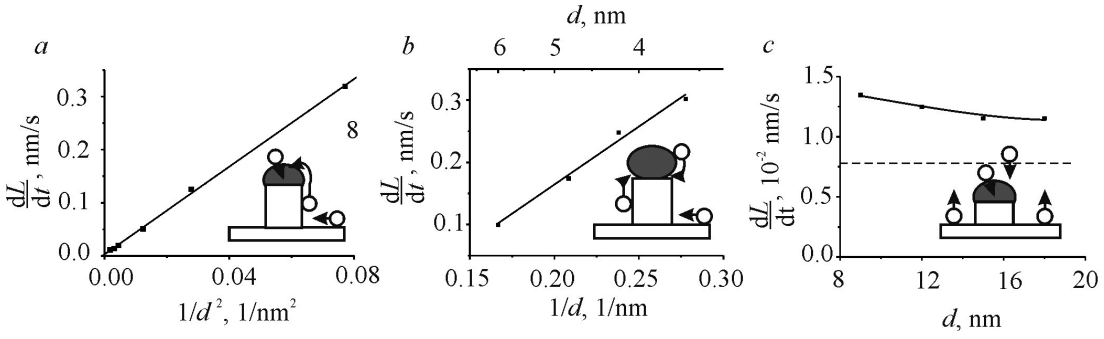


**Fig. 2** Simulated dependences of NW growth rate on catalyst drop size in the diffusion (a,b) and adsorption (c) growth modes at $T$ = 800 K, $F$ = 0.05 ML/s (dashed line corresponds to the external flux $F$).

The character of NW new layer nucleation (mono- or polynucleation) determines the quality of the drop–whisker interface and in turn the further morphology of the growing whisker. The nucleation process at the interface at different temperatures and intensities of deposition flux was studied. Results are presented as $F(T)$ curve where two different regions for mono- and polynucleation are distinguished (Fig. 3a). Area I corresponds to mononuclear and area II to polynuclear growth. The transition from poly- to mononucleation at a given whisker diameter takes place either under temperature increase or under decrease of flux intensity. Figure 3b illustrates nucleus distribution at the drop–NW interface depending on diffusion component contribution in the whisker growth process. When the diffusion component is low, nuclei are randomly distributed at the interface. The increase of diffusion component results in a higher nucleus concentration along the triple line. A similar situation is expected in the case of MBE growth. In Fig. 3c, cross-sections of model NWs grown by CVD and MBE are depicted. The drop–whisker interface after CVD growth is flat contrary to the cup-shaped interface detected during MBE growth condition. Such morphology of whisker–catalyst interface was already experimentally observed [22,23] and can be explained by the influence of the diffusion component of growth on the nucleation process. It should be noted that the higher nuclear concentration along the triple line may be the reason for nanotube-like growth [15,30].

Dependencies of NW growth rate on growth parameters were investigated [37]. At increasing flux intensity the NW growth rate increases with simultaneous enlargement of whisker diameter. The whisker thickening is due to the decrease of adatom diffusion length resulting in island nucleation on the substrate and side-walls of NW. Growth rate dependence on temperature obtained earlier in [37] had two regions with different activation energies: at low temperatures $E_a$ = 0.5 eV and at high temperatures

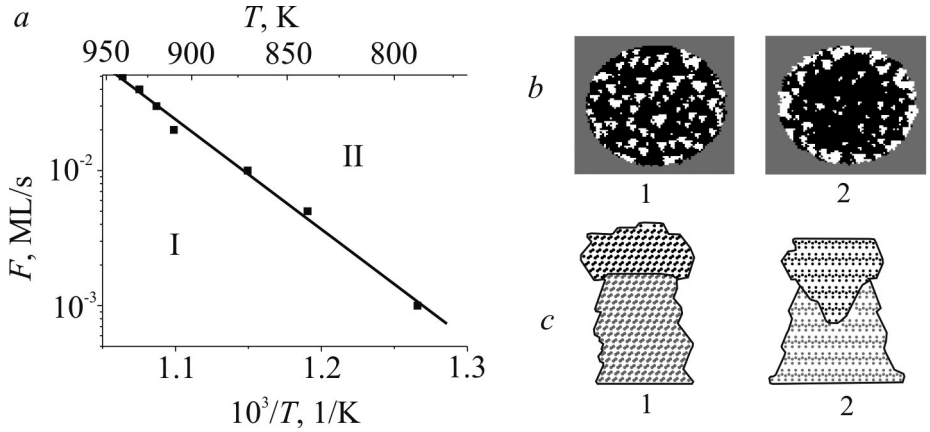


**Fig. 3** (a) Diagram in *F*-*T* coordinates of mono- (I) and polynuclear (II) growth at the drop–whisker interface; (b) plan view cross-sections of drop–whisker interface for low (1) and high (2) diffusion components; (c) cross-sections of NW fragment with catalyst drop after CVD (1) and MBE (2) growth.

$E_a$ = 1 eV. In the low-temperature region, $E_a$ was demonstrated to be close to the activation energy value determined experimentally (0.53 ± 0.02 eV) [22]. Analyses of simulation results revealed that at low temperature, $E_a$ value is sensitive to dissolution of semiconductor material in catalyst drop and at high temperature to material diffusion along the substrate and NW side-walls.

Figure 4 illustrates the branching effect in the model system. In Fig. 4a, images of NW at initial stages of growth are given. At some moment the Au droplet leaves the top of the whisker and initiates growth of the lateral branch. This effect was observed experimentally [15,36]. NW branching may also be due to drop splitting. An example of such a phenomenon is shown in Fig. 4b. Drop splitting may occur for large diameters of catalyst drop and low surface tension of the drop. Drop surface tension is a function of temperature and concentration of semiconductor material in the liquid alloy [38]. Under some growth conditions, the growth front under large drops is no more a (111) facet but several (111)

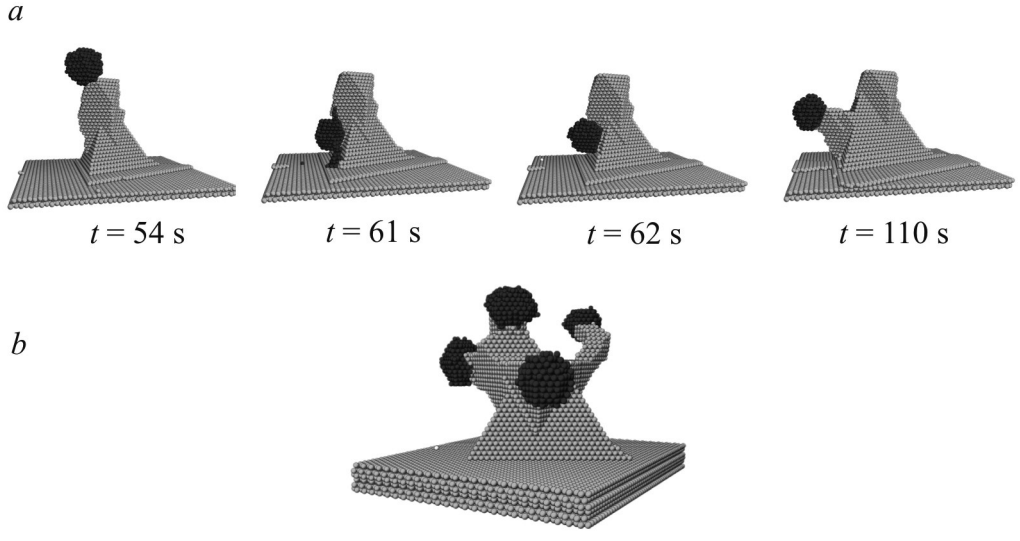


**Fig. 4** 3D image of NWs demonstrating branching effect due to drop migration (a) and drop splitting (b).

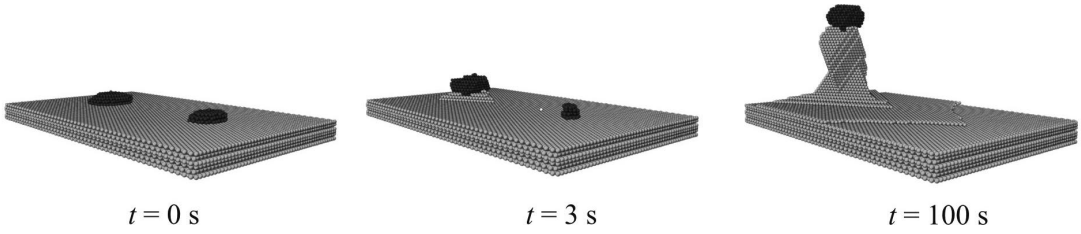


**Fig. 5** Ripening effect in the model system with two catalyst drops of different sizes, 3.0 and 4.2 nm, during NW growth at $T$ = 800 K, $F$ = 0.05 ML/s.

facets. Layer-by-layer growth on each of these facets results in NW branching. The ripening effect was observed in the model system. Figure 5 shows a model substrate with two Au droplets of different size. With increasing time, the large drop merges with the small one and at the final stage only one whisker is growing.

The feasibility of nanotube growth was revealed during morphology examination of NW formation in the incorporation regime. This regime may be dominant at weak wetting and small NW diameters. In this case, the formation of hollow whiskers is possible under certain temperatures and fluxes. Figure 6 demonstrates regions of growth conditions corresponding to different NW morphology. NWs could grow only in a relatively narrow area of temperatures and fluxes. The dashed area corresponds to whiskers with small cavities along their axes. At higher temperatures, growth of solid NWs was observed, and at lower temperatures hollow NWs grew. A scheme for tube-like NW formation could be the following: atoms, incorporated under the drop, form a ring along the triple line which prevents incorporation of matter under the drop. The conditions for nanotube formation are weak wetting between substrate and catalyst materials and a considerable amount of atoms being incorporated along the drop–whisker triple line.

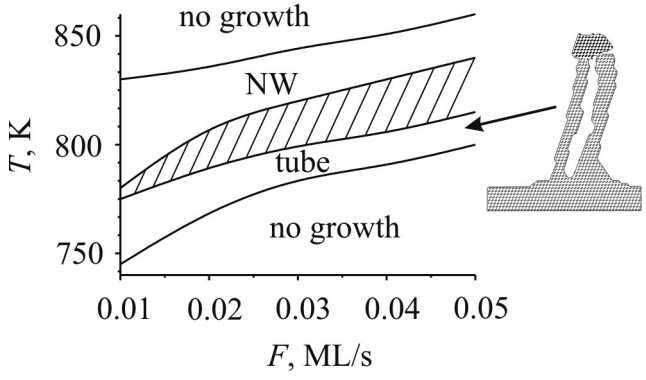


**Fig. 6** Growth conditions of NWs of various morphologies in the $T$-$F$ coordinates ($d$ = 4.8 nm). Dashed region corresponds to NWs with isolated cavities along whisker axes; below is the region of nanotube formation.

The suggested MC model was also used for the analyses of Si–Ge whisker growth. The composition dependence of $Si_{1-x}Ge_x$ NWs on diameter was investigated. As was shown in [39], the composition of $Si_{1-x}Ge_x$ alloy can be dependent not only on growth conditions but on NW diameter as well. The authors of work [39] explained this phenomenon by the Gibbs–Thomson effect. We provide some other explanation for composition dependence on NW size. In Fig. 7a, a 3D view of model whisker grown at simultaneous Si and Ge deposition is shown. For such whiskers, the increase of Ge concentration with

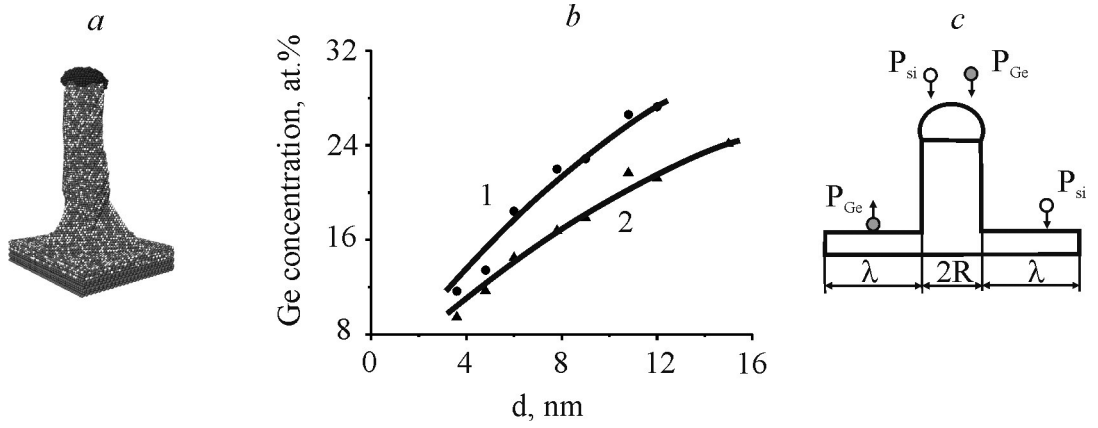


**Fig. 7** $Si_{1-x}Ge_x$ NW growth at $T$ = 750 K and simultaneous Si and Ge deposition ($F_{PSi}$ = 0.01 ML/s; $F_{PGe}$ = 0.005 ML/s): (a) 3D image of NW, Au is marked in black, Si in dark gray, and Ge in light gray color; (b) relationship between Ge concentration in $Si_{1-x}Ge_x$ NW and the diameter of the whisker grown at different temperatures: 1 – $T$ = 750 K, 2 – $T$ = 800 K; (c) schematic view of adsorption and desorption precursor fluxes: white circle – Si-containing precursor ($P_{Si}$), gray circle – Ge-containing precursor ($P_{Ge}$), $R$ – whisker radius, $\lambda$ – Si diffusion length.

enlargement of NW diameter was observed experimentally [39]. Model curves for two growth temperatures in Fig. 7b demonstrate the same dependence. This effect can be explained by different adsorption properties of Si- and Ge-containing precursors ($P_{Si}$ and $P_{Ge}$): if $P_{Ge}$ is adsorbed primary on the drop, and $P_{Si}$, both on the drop and on the substrate, then the Ge percentage in NW will be dependent on drop size. The dependence of Ge content on temperature is due to changing of precursor desorption fluxes with temperature variation. In a limiting case, when Ge precursor is adsorbed only on the drop surface, the Ge percentage in the NW is proportional to $\pi R^2$, and the Si percentage to $\pi(R + \lambda)^2$, where $R$ is the drop radius and $\lambda$ is the diffusion length responsible for Si gathering. In this case, the dependence of Ge content in $_{1-x}Ge_x$ alloy can be estimated as $a{\cdot}\pi R^2/[a{\cdot}\pi R^2 + b{\cdot}\pi\ (R + \lambda)^2]$, where $a$, $b$ are coefficients determined by intensities of Ge and Si fluxes. NW chemical composition has to be carefully considered and controlled because composition determines the NW's characteristics.

## CONCLUSIONS

A kinetic MC model of VLS growth mechanism of NWs was realized. The dependence of NW morphology on growth conditions was studied using this model. The influence of diffusion component of growth on the relief of the interface between catalyst drop and NW was demonstrated. The possibility of tube-like whisker formation was shown. A range of model growth conditions corresponding to NW and nanotube formation was determined. Activation energy of NW growth rate was estimated: at low temperature, the $E_a$ value is sensitive to dissolution of semiconductor material in catalyst drop and at high temperature to material diffusion along the substrate and NW side-walls. The suggested MC model can be used for analysis of NW growth on the base of different materials.

## ACKNOWLEDGMENTS

This work was supported by the Russian Foundation for Basic Research (Grant No. 08-02-00068) and the program of Basic Research of the Presidium RAS (N 27.30, project 1.13.13).

 

## REFERENCES


1. E. I. Givargizov. *Crystallogr. Rep.* **51**, 888 (2006).
2. O. Hayden, R. Agarwal, W. Lu. *Nano Today* **3**, 12 (2008).
3. X. Jiang, Q. Xiong, S. Nam, F. Qian, Y. Li, C. M. Lieber. *Nano Lett.* **7**, 3214 (2007).
4. J. Xiang, W. Lu, Y. Hu, Y. Wu, H. Yan, C. M. Lieber. *Nature* **441**, 489 (2006).
5. Y. C. Cui, Q. Wei, H. Park, C. M. Lieber. *Science* **293**, 1289 (2001).
6. G. Zheng, F. Patolsky, Y. Cui, W. U. Wang, C. M. Lieber. *Nat. Biotechnol.* **23**, 1294 (2005).
7. F. Patolsky, B. P. Timko, G. Zheng, C. M. Lieber. *MRS Bull.* **32**, 142 (2007).
8. R. S. Wagner, W. C. Ellis. *Appl. Phys. Lett.* **4**, 89 (1964).
9. T. I. Kamins, R. S. Williams, D. P. Basile, T. Hesjedal, J. S. Harris. *J. Appl. Phys*. **89**, 1008 (2001).
10. A. I. Persson, M. W. Larsson, S. Stenstrom, B. J. Ohlsson, L. Samuelson, L. R. Wallenberg. *Nat. Mater.* **3**, 677 (2004).
11. D. P. Yu, Y. J. Xing, Q. L. Hang, H. F. Yan, J. Xu, Z. H. Xi, S. Q. Feng. *Physica E* **9**, 305 (2001).
12. R. Q. Zhang, Y. Lifshitz, S. T. Lee. *Adv. Mater.* **15**, 635 (2003).
13. J. Kikkawa, Y. Ohno, S. Takeda. *Appl. Phys. Lett*. **86**, 123109 (2005).
14. H. Jagannathan, M. Deal, Y. Nishi, J. Woodruff, C. Chidsey, P. C. McIntyre. *J. Appl. Phys*. **100**, 024318 (2006).
15. C. Yan, M. Y. Chan, T. Zhang, P. S. Lee. *J. Phys. Chem. C* **113**, 1705 (2009).
16. W. Seifert, M. Borgstrom, K. Deppert, K. A. Dick, J. Johansson, M. W. Larsson, T. Martensson, N. Skold, C. P. T. Svensson, B. A. Wacaser, L. R. Wallenberg, L. Samuelson. *J. Cryst. Growth* **272**, 211 (2004).
17. L. Gao, R. L. Woo, B. Liang, M. Pozuelo, S. Prikhodko, M. Jackson, N. Goel, M. K. Hudait, D. L. Huffaker, M. S. Goorsky, S. Kodambaka, R. F. Hicks. *Nano Lett.* **9**, 2223 (2009).
18. A. M. Morales, C. M. Lieber. *Science* **279**, 208 (1998).
19. B. A. Wacaser, M. C. Reuter, M. M. Khayyat, C.-Y. Wen, R. Haight, S. Guha, F. M. Ross. *Nano Lett.* **9**, 3296 (2009).
20. K. Kang, D. A. Kim, H.-S. Lee, C.-J. Kim, J.-E. Yang, M.-H. Jo. *Adv. Mater*. **20**, 1 (2008).
21. T. Baron, M. Gordon, F. Dhalluin, C. Ternon, P. Ferret, P. Gentile. *Appl. Phys. Lett*. **89**, 233111 (2006).
22. S. Kodambaka, J. Tersoff, M. C. Reuter, F. M. Ross. *Phys. Rev. Lett*. **96**, 096105 (2006).
23. N. Zakharov, P. Werner, L. Sokolov, U. Gosele. *Physica E* **37**, 148 (2007).
24. K. Lew, J. M. Redwing. *J. Cryst. Growth* **254**, 14 (2003).
25. W. Park, G. Zheng, X. Jiang, B. Tian, C. M. Lieber. *Nano Lett.* **8**, 3004 (2008).
26. M. C. Plante, R. R. LaPierre. *J. Cryst. Growth* **286**, 394 (2006).
27. P. Madras, E. Dailey, J. Drucker. *Nano Lett.* **9**, 3826 (2009).
28. K. A. Dick, S. Kodambaka, M. C. Reuter, K. Deppert, L. Samuelson, W. Seifert, L. R. Wallenberg, F. M. Ross. *Nano Lett*. **7**, 1817 (2007).
29. D. Wang, F. Qian, C. Yang, Z. Zhong, C. M. Lieber. *Nano Lett.* **4**, 871 (2004).
30. E. P. A. M. Bakkers, M. A. Verheijen. *J. Am. Chem. Soc*. **125**, 3440 (2003).
31. M. Nolan, S. O'Callaghan, G. Fagas, J. C. Greer, T. Frauenheim. *Nano Lett*. **7**, 34 (2007).
32. T. Vo, A. J. Williamson, G. Galli. *Phys. Rev. B* **74**, 045116 (2006).
33. V. G. Dubrovskii, N. V. Sibirev. *J. Cryst. Growth* **304**, 504 (2007).
34. I. G. Neizvestny, N. L. Shwartz, Z. Sh. Yanovitskaya, A. V. Zverev. *Comput. Phys. Commun.* **147**, 272 (2002).
35. A. V. Zverev, K. Yu. Zinchenko, N. L. Shwartz, Z. Sh. Yanovitskaya. *Nanotechnol. Russia* **4**, 215 (2009).
36. E. I. Givargizov. *J. Cryst. Growth* **31**, 20 (1975).
37. A. G. Nastovjak, I. G. Neizvestny, N. L. Shwartz. *Solid State Phenomena* **156–158**, 235 (2010).
38. D. Bahloul-Hourlier, P. Perrot. *J. Phase Equilib. Diffusion* **28**, 150 (2007).


 

39. X. Zhang, K.-K. Lew, P. Nimmatoori, J. M. Redwing, E. C. Dickey. *Nano Lett*. **7**, 3241 (2007).

 